Circulation type classification derived on a climatic basis to study air quality dynamics over the Iberian Peninsula

Running head: Circulation type classification for air quality applications.

Víctor Valverde[a], María T. Pay[a,b], José M. Baldasano[a,c]

[a]Earth Sciences Department, Barcelona Supercomputing Center-Centro Nacional de Supercomputación, Barcelona, Spain.

[b]Laboratoire de Météorologie Dynamique, École Polytechnique, 91128 Palaiseau Cedex, France

[c]Environmental Modeling Laboratory, Technical University of Catalonia, Barcelona, Spain.

victor.valverde@bsc.es, maria.pay@bsc.es, jose.baldasano@bsc.es

*Corresponding author: victor.valverde@bsc.es. Earth Science Department, Barcelona Supercomputing Center-Centro Nacional de Supercomputación (BSC-CNS). Jordi Girona 29, Edificio Nexus II, 08034 Barcelona, Spain. Tel.: +34 93 413 75 81; Fax: +34 93 413 77 21

Abstract

A circulation type classification is derived for the 1983-2012 climatic period in order to characterize air quality dynamics over the Iberian Peninsula (IP). Sensitivity tests to automatic classification techniques and other factors affecting the classification (number of patterns, temporal and spatial resolution, domain size, etc.) are performed in order to objectivize the set-up that maximizes its quality. The ERA-Interim reanalysis and the cost733class classification software are used. The identified circulation types (CTs) are described in terms of frequency, persistence, transitions, and location of isobaric systems. The temporal stability of the classification is evaluated following a cross-validation process that compares the results of the climatic and yearly classifications, leading to the identification of a representative year. Moreover, a representative day for each CT is identified using an objective score that minimizes the absolute value difference of the daily grid with respect to the average CT grid. The reference set-up uses a cluster-based technique (Ck-means) on a daily mean sea level pressure database. Six CTs are identified which are consistent with synoptic patterns found in the literature. Furthermore, the CTs of the climatic period are temporally stable showing similar characteristics in terms of frequency and location of high and low pressure systems as those of the representative year (2012). As a first application of the circulation type classification, 1h-maximum NO_2 concentration maps from the CALIOPE Air Quality Forecasting System are analysed for the representative days. Synoptic circulation controls the origin and strength of advection explaining transport and NO_2 background concentration over the IP. However, there is a strong spatial heterogeneity: in the central, northern, and southern IP, NO_2 concentrations are controlled by the synoptic circulation, whereas in Spanish Mediterranean coastal areas a combination of synoptic and mesoscale dynamics explains the NO_2 concentration patterns.

Keywords: climate; synoptic classification; circulation types; air quality; NO_2; COST733; ERA-Interim

1 Introduction

Air quality depends on emissions, both natural and anthropogenic, meteorology, and the topographical characteristics of the area under study (Baldasano *et al*., 1994; Seinfeld and Pandis, 2006). At the local scale natural emissions depend on temperature and humidity. Transport relies on wind characteristics and vorticity. Photochemistry is determined by temperature, humidity, and solar radiation. Precipitation influences deposition (wet removal), and topography controls mesoscale dynamics such as land-sea breezes and mountain-valley winds. Furthermore, atmospheric circulation at the synoptic scale affects pollution transport at the regional scale (Flocas *et al*., 2009). Therefore, in order to characterize air quality in a given territory, it is necessary to understand the role of the synoptic circulation controlling its regional and local dynamics (Elminir, 2005; Giorgi and Meleux, 2007; Demuzere *et al*., 2009).

In recent years correlations between air quality and specific synoptic patterns or CTs have been studied. Demuzere *et al.* (2009) provides insight in regional meteorological processes that play a role in O_3 formation at four mid-latitude sites in the Netherlands. Shreshta *et al*. (2009) and Zhang *et al*. (2013) reveal that under the influence of CTs with high wind speed, low O_3 concentrations were registered in Southeast Asia, whereas with weak synoptic winds high O_3 concentrations were registered. Ganor *et al*. (2010) relates the occurrence of mineral dust outbreaks in the Eastern Mediterranean to the presence of thermal low pressure areas over Maghreb. In the IP under anticyclonic conditions mesoscale phenomena control O_3 during summer along the Spanish Mediterranean coast (Millán *et al*., 1997; Barros *et al*., 2003; Gonçalves *et al*., 2009; Castell-Balaguer *et al*., 2012). In summer under a blocking anticyclone over Central Europe, there is a net transport of O_3 and precursors towards NW Spain that increases surface O_3 concentration (Saavedra *et al*. 2012). Exceedances of PM10 limit value have been related to the transport of mineral dust from the Sahara, especially in late spring when a deep low is centred over the Western Portuguese coast, and in summer when a high pressure system is formed to compensate a thermal low at the surface over Algeria (Salvador *et al*. 2008, Salvador *et al*., 2013).

Synoptic classifications enable the establishment of discrete CTs by categorizing the continuum of atmospheric circulation based on their similarities (Beck and Philipp, 2010, Philipp *et al*., 2014). The European Cooperation in Scientific and Technology Action 733 (COST733) harmonised classification techniques over Europe (Philipp *et al*., 2010) in three groups: subjective, automatic and hybrid. Automatic techniques based on statistical methods find patterns within the input data and assign samples (days) to the identified CTs in a systematic and objective way, although their configuration critically affects the results (Philipp *et al*., 2014).

Several synoptic classifications have already been derived over the IP (or areas within) for different purposes. This include atmospheric transport characterization (Petisco, 2003; Rasilla, 2003; García-Valero *et al*., 2012), wind analysis (Azorin-Molina *et al*., 2009; Jiménez *et al*., 2009), precipitation trend (Romero *et al*., 1999; Casado *et al*., 2010; Casado and Pastor, 2013), snowfall variability (Esteban *et al*., 2005), lightning activity (Pineda *et al*., 2010), desert dust intrusions (Alonso-Pérez *et al*., 2011; Salvador *et al*., 2013), and transport of pollutants (Saavedra *et al*., 2012, Russo *et al*., 2014).

The present work aims to obtain an objective and automatic synoptic classification over the IP on a climatic basis (1983-2012) to enable further air quality dynamics characterization (Fig. 1). Sensitivity analyses are first performed to several classification techniques and other factors affecting the classification to identify a reference set-up. Second, the resulting CTs are characterized. The synoptic classification is evaluated in terms of its temporal stability, which allows the identification of the most representative year during the climatic period. Kinematic back-trajectories obtained by means of the HYbrid Single-Particle Lagrangian Integrated Trajectory model (HYSPLIT, Draxler and Rolph, 2013) are used to confirm the resulting CTs. Finally, as a first application of the synoptic classification, a characterization of NO_2 dynamics over Spain is performed through analysis of NO_2 concentration maps from the CALIOPE Air Quality Forecasting System (CALIOPE-AQFS) (www.bsc.es/caliope) on representative days of CTs.

The paper is organized as follows. Section 2 describes the methods and data used to derive and evaluate the synoptic classification, and to define a representative year and representative days. Section 3 shows the results of the sensitivity analyses and the characteristics of the identified CTs, the temporal stability of the classification, the comparison with the back-trajectories, and the analysis of NO_2 dynamics. Finally, conclusions are given in Section 4.

2 Methods

A synoptic classification is sensitive not only to the classification technique (clt) but also to other factors as the number of CTs considered (nCT) (Michelangeli *et al*., 1995; Philipp *et al*., 2007; Fereday *et al*., 2008, Philipp *et al*., 2014), the large-scale input meteorological variable used as proxy (iv) (Casado and Pastor, 2013) , the vertical level of the input meteorological variable (vl) (Erpicum *et al*., 2008), the temporal resolution (tr) (Casado and Pastor, 2013), performing an annual or seasonal classifications (se) (García-Valero *et al*., 2012), the horizontal resolution (hr), and the domain size (d) (Jiménez *et al*., 2009; Demuzere *et al*., 2009; García-Bustamante *et al*., 2012, Beck *et al*., 2013). Sensitivity tests have been performed to identify the most objective set-up

114 possible for the synoptic classification used in the air quality characterization (Table 1). 115 The software used to derive the classifications is the open source cost733class software 116 version 1.2. It was developed during the COST733 Action for easily creating, 117 comparing and evaluating classifications (Philipp *et al*., 2014).

118 The analyses cover the climatic period of 1983-2012 and use ERA-Interim reanalysis 119 data (Dee *et al*., 2011; http://apps.ecmwf.int/datasets/data/ interim_full_daily/) from the 120 European Centre for Medium-Range Weather Forecasts (ECMWF). The reanalysis 121 dataset provides reliable gridded meteorological variables over a global domain every 122 six hours, at several horizontal resolutions, both at the surface and staggered at 37 123 vertical levels up to 1 hPa geopotential height.

124 An optimum classification maximizes the separability of the identified CTs while 125 minimizing the within-type variability. The Explained Variation (EV) index is a 126 measure of the classification quality (Eq. 1). EV is the result of the ratio between the 127 internal variance of all the CTs (WSS) and the total variance of all the elements without 128 clustering (TSS). WSS is the distance among samples in one CT calculated as within 129 CT sum of squares (Eq. 2), and TSS is the total sum of squared differences between all 130 elements and the overall mean.

$$\text{EV} = 1 - (\text{WSS}/\text{TSS}) \quad (1)$$

$$WSS = \sum_{j=1}^{k} \sum_{i \in CT_j} D(X_i, \bar{X}_j)^2 \quad (2)$$

131 In Eq. 2, k is the number of CTs, CT_j is the j of the k CTs, and D is the Euclidean 132 distance between the sample (X_i) and its CT centroid ($\bar{X}_j$). The Euclidean distance is 133 calculated considering the meteorological variable used in the classification on all grid

cells. The sensitivity analyses are evaluated through the EV, which ranges from 0 to 1. CTs are more meaningful in terms of explaining the original amount of information when EV is closer to 1. According to Demuzere *et al*. (2011), the choice of an appropriate circulation type classification should be based on an objective evaluation of the explanatory power of the CTs on the region they are derived for and the purpose of the classification. Therefore in this research, the choice of the configuration has been done attending not only to the quality of the classification (expressed by the EV) but also to its main purpose, which is the identification of typical CTs to study their influence on air quality dynamics over the IP.

The Rand Index (RI) is used as a measure of the agreement between two classifications with the same or a different number of CTs (Rand, 1971). RI ranges from 0 to 1. High values of RI imply that the identified CTs are similar in both classifications.

The identified CTs are characterized by describing the atmospheric dynamics from a synoptic point of view. The description includes the relative location of the action centres, which determine the direction and speed of air masses both at the surface and 500 hPa geopotential height (Z500). Z500 is situated at a level which the weight of the air column above and below it are alike enabling an estimation of the vertical structure of the atmosphere. Moreover, a quantitative description of each CT is given including the climatic frequency, the monthly distribution, the transitions between CTs which is useful for predictability at medium term (James, 2007), and the mean and maximum persistence. Cahynová and Huth (2009) defined persistence as the length of a sequence of days that are classified with one CT, while preceded and succeeded by another CT.

A temporally stable synoptic classification is able to identify similar CTs when using meteorological databases for different periods. An evaluation of the temporal stability of the classification is performed following a cross-validation process similar to that used in Fereday *et al*. (2008) and García-Valero *et al*. (2012). The synoptic classification of each year is compared to the 1983-2012 classification. The total stability is defined as the percentage of days within the year that are classified in the same CT in both classifications. Higher total stability indicates more similar results between the yearly and the 1983-2012 circulation type classifications. The year with the highest stability is selected as the representative year.

To confirm the consistency of CTs with the main sources of air masses directed towards the IP (Martín-Vide and Olcina, 2001), a comparison with ensemble back-trajectories on a representative day of each CT is performed. To adequately sample the history of the mass, the HYSPLIT model is used to determine 60-h back-trajectories ending at several locations (Madrid, Barcelona, Seville, Bilbao, Zaragoza, Santiago de Compostela and Palma de Mallorca, Fig. 2a). The ensemble back-trajectories (27 members) are derived at 1500 and 5500 magl (approximately equivalent to Z850 and Z500, respectively) using the global reanalysis database Global Data Assimilation System (on a 1º x 1º grid) from National Centers for Environmental Prediction.

To objectively select a representative day for each CT, a daily score is designed to minimize the differences between the daily grid and the average grid of a given CT. For each day (t) within a given CT, the Day Score (DS) is calculated as the sum of the absolute value of the differences between the daily value and the average value of the meteorological variable of the CT for each cell (i) of the grid (Eq. 3).

$$DS_t = \sum_{i=1}^{n} |v_{t,i} - \overline{v_i}| \qquad (3)$$

In Eq. 3, n is the number of cells of the grid; and $\overline{v_i}$ is the arithmetic mean of the input variable on each i cell of the domain for all days belonging to the CT. The Representative Day Score (*RDS*) minimizes the value of the DS identifying the representative day for each CT (Eq. 4).

$$RDS = \min(DS_t) \qquad (4)$$

The RDS is a spatially explicit score useful to rank all days belonging to a given CT according to their similarity to the average value of the input variable of the 1983-2012 period. In addition, an extra criterion is established for the selection of the representative day. The day selected as representative has to be a day belonging to the month in which the CT is most frequent in the climatic period.

Furthermore, NO_2 dynamics over the IP are analysed on the representative day of each CT. NO_2 concentration maps are provided by the CALIOPE-AQFS, which operationally provides 48-h forecast concentrations of main pollutants over the IP at high spatial (4 km x 4 km) and temporal resolution (1h). CALIOPE-AQFS is described and evaluated in detail elsewhere (Baldasano *et al.*, 2008, 2011; Pay *et al.*, 2011, Pay *et al.*, 2012, Pay *et al.*, 2014). Briefly, it integrates the fully compressible, Eulerian and nonhydrostatic Weather Research and Forecasting Model which uses the advanced research dynamical solver, WRF-ARWv3.0.1 (Skamarock and Klemp, 2008), an emission model (HERMESv2; Guevara *et al.*, 2013), the Community Multi- scale Air Quality model (CMAQv4.5; Byun and Schere, 2006), and a mineral dust atmospheric model (BSC-DREAM8b; Pérez *et al.*, 2006a, Pérez *et al.*, 2006b; Basart *et al.*, 2012) together in an air quality forecast system. CALIOPE-AQFS is evaluated in near-real time against air quality observations from more than 400 ground-level stations from the Spanish monitoring network.

A short description of the configuration of the meteorological driver is given considering its strong influence on the dynamics of NO_2 concentration. First, WRF-ARW runs over Europe (the mother domain) at 12 km x 12 km horizontal resolution using initial and boundary conditions from the Global Forecast System (GFS/FNL) dataset with 6-h temporal resolution and 0.5º x 0.5º horizontal resolution. Over IP, WRF runs at higher resolution (4 km x 4 km) by means of a one-way nesting over the mother domain. Vertically, WRF-ARW is configured with 38 σ vertical levels from the surface up to 50 hPa, with 11 levels characterizing the planetary boundary layer. The parameterizations used are as follows: WSM 3-class microphysics scheme, Kain-Fritsch Eta convective scheme, RRTM long-wave radiation, simple short wave radiation, Monin-Obukhov similarity surface layer physics, Noah Land Surface Model, and YSU planetary boundary scheme.

Concerning the CALIOPE-AQFS performance, the system was fully evaluated over the IP domain for a full year (2004) for both meteorology and air quality (Baldasano *et al.*, 2011 and its supplementary material). Good performance was found for wind speed and wind direction with mean absolute error ~1.7 m s^{-1} and ~48º, respectively. The WRF model tends to overestimate surface wind speed, although the mean bias error remains below 0.8 m s^{-1} during summertime and around 0.9 m s^{-1} in winter. The CALIOPE-AQFS is able to reproduce NO_2 concentration as shown by statistics (Mean Bias, MB; Root Mean Square Error, RMSE; correlation coefficient, r) calculated on an hourly basis. Although NO_2 tends to be under estimated (MB = -12.3 μg m^{-3}) the general dynamics are well captured (r = 0.53). The highest errors are found in urban stations (RMSE = 33.6 μg m^{-3}) and lowest in rural ones (RMSE = 7.6 μg m^{-3}).

3 Results

3.1 Determination of the reference synoptic classification set-up

Sensitivity tests to the classification technique and other factors affecting the results of the classification are performed (Table 1). Each test is run on a climatic basis (1983-2012) and evaluated in terms of EV. Within-type Standard Deviation and the Fast Silhouette Index are other metrics that inform about the classification quality. The results of these metrics are convergent with the EV and are presented as supplementary material (S1). The analyses are run with only one factor varying each time.

3.1.1 Classification technique

Test one (Table 1) analyses the effect of the automatic technique considered on the synoptic classification quality. The automatic techniques included in the cost733class software belong to three families of classification techniques: (1) correlation techniques, (2) Principal Component Analysis (PCA), and (3) clustering techniques. The techniques differ depending on the multivariate statistics used. A complete explanation of the 12 techniques used, their acronyms, and their implementation in the cost733class software is presented in Philipp *et al*. (2014) and references therein.

On average, cluster techniques have 15% and 60% higher EV than PCA techniques and correlation techniques respectively. The classification techniques that present the highest EV are the non-hierarchical clustering techniques (as in Casado and Pastor, 2013) (Fig. 3a). Several variants of the k-means clustering (KMN, CKM and DKM), rank the highest EV together with the Simulated ANealing and Diversified Randomization (SAN). The k-means clustering has been widely used to derive synoptic classifications (Romero *et al*., 1999; Rasilla, 2003; Jiménez *et al*., 2009). KMN uses random seeds for the initialization of the clustering process, which can lead to suboptimum classifications. In contrast, CKM and DKM use the most dissimilar seeds possible (calculated in a previous step of the classification), enabling an optimum clustering. Unlike DKM, CKM does not allow the creation of CTs with less than 5% of the original data, in order to avoid the creation of extreme or infrequent CTs. As this work aims to obtain CTs that are related to the most common air quality patterns CKM is chosen. SAN is a clustering technique that has performed better than CKM in classifications made by other authors (Philipp *et al*., 2007; Fereday *et al*., 2008). In this case CKM and SAN perform similarly (EV = 0.474 and 0.478, respectively). Based on the higher computational cost of running classifications with SAN compared to CKM, the latter is chosen as the reference classification technique.

The robustness of the identified CTs between classification techniques is evaluated by means of the RI. The highest similarity is observed between all techniques based on k-means (RI> 0.88 on average; CKM and DKM rank RI = 0.99) (Fig. 4). With respect to CKM, PCA-based techniques range from 0.71 (PTT) to 0.79 (PXE), whereas correlation-based techniques range from 0.63 (ERP) to 0.78 (LND). These results indicate that k-means techniques determine similar CTs and reinforce the decision to use CKM as the classification technique.

3.1.2 Number of circulation types

Test two (Table 1) studies the effect of the number of CTs on the synoptic classification quality. In general terms, EV increases with the number of CTs, but the increase is not linear (Fig. 3b). The number of CTs should be a balance between the EV and having an appropriate number of situations for air quality characterizations. For cluster techniques there is not a specific criterion to select the reference number of CTs. A 5% increase threshold in the EV is established to determine the most appropriate number of CTs. This leads to consider six CTs. Considering CKM, the EV is 0.48 using 6 CTs and 0.50 using 7 CTs. A complete table with the EV values is shown in the supplementary material (S2). The obtained value of EV using CKM and six CTs is in the same range to those obtained by García-Valero *et al*. (2012) for a seasonal classification over Spain.

3.1.3 Meteorological variable used as proxy

Test three (Table 1) evaluates the effect of using different large-scale meteorological variables as a proxy on synoptic classification. Several classifications use the mean sea level pressure (mslp) as proxy meteorological variable because it is useful for relating the classification to variables influenced directly by the low levels of the atmosphere like surface temperature (Philipp *et al*., 2007; Cassou *et al*., 2005; Yiou *et al*., 2008), sea surface temperature (Fereday *et al*., 2008), wind (Jiménez *et al*., 2009) and air quality.

Five meteorological variables (iv) available in the ERA-Interim database are tested: mslp, 10-meter wind components (UV10), 1000-hPa vorticity (Vort1000), 2-meter air temperature (T2m) and relative humidity (RH). T2m shows the highest EV (0.80), followed by mslp (EV = 0.48), RH (EV = 0.40) and UV10 (EV = 0.26) (Fig. 3c). Similar results are obtained when using KMN, DKM, and SAN (Supplementary material – S3). An analysis (not shown here) of the annual distribution of the identified CTs using T2m as meteorological variable indicates that the identified CTs were more related to seasonality than to atmospheric circulation. Thus, mslp is chosen as the meteorological reference variable. Atmospheric pressure is valuable because it provides information about the stability/instability of the atmosphere and the wind speed and direction, critical features to understand pollution transport dynamics.

3.1.4 Vertical level

Test four (Table 1) examines the effect of the vertical level on the classification quality. Surface data have typically been used to derive classifications (Kirchhofer 1974; Yiou and Nogaj 2004; Casado *et al*., 2010). To a lesser extent, the geopotential height at 500 hPa (Z500) and 850 hPa (Z850) have been used in other studies (Kruizinga, 1979; Erpicum *et al*., 2008; Casado and Pastor, 2013).

Classifications are obtained at different altitudes from 1000 hPa to 1 hPa by 100 hPa increments. EV increases from the surface to upper vertical levels (Fig. 3d). Below 850 hPa the atmospheric circulation is strongly influenced by the topography, leading to complex and diverse pressure patterns to classify (EV~ 0.48). At higher vertical levels where the complexity of the atmospheric circulation is lower, the identification of CTs is easier (higher EV). Many processes involved in air quality dynamics (emission, diffusion, advection, chemistry, deposition, etc.), together with effects of pollution on human health and the environment occur within the lower troposphere. Although ranking as the lowest EV (0.48), the reference vertical level is established at the surface (mslp), considering that the purpose of this synoptic classification is to identify CTs for air quality dynamics characterization.

3.1.5 Temporal resolution

Test five (Table 1) studies the impact of the temporal resolution. ERA-Interim reanalysis provides data every 6 hours (00:00, 06:00, 12:00, and 18:00 UTC).

Resolutions used in the classification are 24-h (at 12:00 UTC), 12-h (using data at 00:00 and 12:00 UTC), 6-h (at 00:00, 06:00, 12:00 and 18:00 UTC) and 06-h mean (mean of 00:00, 06:00, 12:00 and 18:00 UTC). Results show that EV does not significantly change with the increase of the temporal resolution (Fig. 3e), with EV = 0.48 for both 6-h and 12-h resolution. On the other hand, results show a very slight improvement in the classification quality when using the 6-h mean (EV = 0.49). However, in order to reduce the computational cost of the classification the reference temporal resolution is set to 24-h.

3.1.6 Seasonal classification

Test six (Table 1) evaluates the impact of considering either seasonal or annual data on the classification quality. Winter and autumn EV are 14% and 5% higher than the annual EV, respectively (Fig. 3f). However, spring (EV= -2%) and summer (EV = -1%) are in the same range of quality as the annual classification. Overall, the mean seasonal EV is 0.019 higher than the annual EV.

An annual synoptic classification is chosen considering that a reduced number of CTs is desirable to facilitate the air quality dynamics characterization and that the total increase of seasonal EV respect to the annual classification EV is less than 4%.

3.1.7 Horizontal resolution

Test seven (Table 1) studies the impact of the horizontal resolution of the input data on the classification quality. Five resolutions 0.125º x 0.125º (110467 cells), 0.25º x 0.25º (27784 cells), 0.75º x 0.75º (3162 cells), 1.5º x 1.5º (864 cells), and 3º x 3º (238 cells), are considered. A higher resolution enables the description of more complex dynamics but may hinder the identification of CTs by introducing complexity to the input database.

Overall, horizontal resolution has a low impact on the EV (Fig. 3g). For resolutions higher than 0.75º x 0.75º the increase in EV is less than 1%, whereas lower resolutions decrease the EV by 2.6% (1.5º x 1.5º) and 3.1% (3º x 3º). The 0.75º x 0.75º resolution guarantees high classification quality with fewer data, reducing the computational cost and storage requirements. It requires only 3% of the storage requirements compared to the 0.125º x 0.125º classification.

3.1.8 Domain size

Test eight (Table 1) analyses the effect of domain size on the classification quality. Three spatial domain sizes (D00 = 28x10^6 km^2; D01 = 15x10^6 km^2; D02 = 5x10^6 km^2) centred over the IP have been studied (Fig. 2a).

Results indicate that EV significantly varies with the domain size, with the highest EV at D02 (0.62) and the lowest at D00 (0.41) (Fig. 3h). The increase in EV when considering D02 instead of D01 is almost 30%. This result is due to the fact that within a smaller domain the heterogeneity of atmospheric circulation is lower than in bigger domains, leading to an easier identification of CTs (Beck and Philipp, 2010). Similar results are obtained by Beck *et al*. (2013) when analysing the influence of the domain size on the classification quality, using 8 domains from 0.77x10^6 to 18.5x10^6 km^2.

The analysis of the spatial, temporal, and dynamic characteristics of the identified CTs over the different domains indicates that the domain size exerts an important influence on the results of a synoptic classification. For instance, around 50% of the days belonging to a given CT on D01 are not classified on the same CT on D02. This lack of consistency on the classification results between both domains indicates that the identified CTs are domain dependent.

D01 is the most suitable domain for this synoptic classification because it contains the usual locations of the more relevant action centres that affect the transport of air masses towards the IP (Martín-Vide and Olcina, 2001). The IP is greatly affected by the position of the Azores high and the British Isles low, which determine flows from the North-eastern Atlantic Ocean, the Western Mediterranean, Northern Africa, and Northern and Western Europe (all of them included in domain D01). Domain D00 also considers these areas but it ranks lower (EV =0.41) than D01, and is therefore less advisable as a reference domain.

3.1.9 Summary of the reference set-up

According to the results of the eight sensitivity tests, the reference set-up for the circulation type classification uses the cluster-based CKM classification technique on 24-h (12:00 UTC) mean sea level pressure data with a horizontal resolution of 0.75º x 0.75º. The classification is performed without seasonalization on the intermediate D01 domain. Six CTs explain 48% of the 1983-2012 synoptic circulation variability.

3.2 Characterization of circulation types

This section characterises the six synoptic CTs identified for 1983-2012 with the reference set-up (Fig. 5, Table 2).

CT1 is the most frequent CT overall (23.9% of the climatic frequency), especially common in summertime. Two action centres determine the surface pressure structure over Western Europe. They are the Azores high (~1020 hPa) and a low pressure system (~1008 hPa) over Scandinavia (Fig. 5a). Between them isobars are arranged in a NW-

SE orientation enabling the arrival of NW advection to the north of the IP. This synoptic situation leads to atmospheric instability and relative low pressure areas (~1012 hPa) over the Balearic Islands and the Spanish Mediterranean coast. The Cantabrian coast (north of IP) has high mslp (1016 hPa). At Z500, the geopotential isolines are in W-E direction and describe a slight through over Western Europe. This atmospheric situation leads to arctic maritime advection from the West of the British Isles towards the IP (Martín-Vide and Olcina, 2001).

CT2 is the second most frequent CT (22.4%). The intense solar radiation over the IP in summer leads to the formation of a thermal low (Millán *et al*., 1991) (Fig. 5b). CT2 is characterized by a reduced surface pressure gradient over the IP and Western Europe (~1016-1018 hPa), which enable the development of mesoscale processes such as land-sea and mountain-valley breezes, especially along the Spanish Mediterranean coast (Baldasano *et al*., 1994; Millán *et al*., 1997; Azorin-Molina *et al*., 2009). At Z500 there is a moderate geopotential height ridge that affects Western Europe enabling tropical continental advection from Northern Africa towards the IP (Martín-Vide and Olcina, 2001) (Fig. 2b). CT2 is usually replaced by CT1 which is the most frequent summer pattern, and vice versa. CT2 corresponds with the S2 pattern (stagnant situation with SW circulation aloft) of the pseudo-subjective classification by García-Valero *et al*. (2012).

CT3 takes place evenly throughout the year (21.3%) but it is more frequent at the end of winter and during spring (Table 2). CT3 is associated with a blocking anticyclone located over the North Sea that affects the entire domain (Fig. 5c). There are high isobaric patterns over Central Europe (> 1024 hPa), as well as in the IP (1020 hPa), leading to an E-NE advection towards the IP. It is usually replaced by CT2 when the

408 high pressure subsides. At Z500 the 5580 m isoline describes a geopotential height
409 ridge that descends longitudinally from the British Isles to the IP. This situation
410 provokes an arctic continental advection from NE Europe to the IP (Martín-Vide and
411 Olcina, 2001).

412 CT4 accounts for 12% of the climatic frequency and typically occurs during the end of
413 autumn and wintertime. CT4 is characterized by high surface pressure (1024-1030 hPa)
414 over the IP derived from the presence of the Azores high over the Cantabrian Sea (Fig.
415 5d). CT4 determines the arrival of Atlantic air masses to the Cantabrian coast. The
416 north, centre and eastern IP are dominated by the influence of N and NE winds. The
417 geopotential height field structure at 500 hPa is similar to that at the surface showing an
418 air flow reaching the northern and central IP with a maritime origin. However, in the
419 south-western IP air masses have a southern origin. CT4 is usually replaced by CT6 in
420 which the Atlantic advective features are more stressed. CT4 corresponds with the A1
421 pattern (anticyclone over the IP at all vertical levels) derived in García-Valero *et al.*
422 (2012).

423 CT5 typically occurs during transitional seasons (spring and autumn), although it is the
424 second least frequent CT (10.4%). The Azores high (~1020 hPa) is in contrast to a low
425 pressure area (~996 hPa) centred over western Ireland that affects Western Europe,
426 leading to atmospheric instability over the IP (Fig. 5e). A horizontal pressure gradient is
427 established from NW (~1008 hPa) to SE (~1016 hPa) over the IP, enabling maritime
428 advection towards western IP, as described by Martín-Vide and Olcina (2001). At Z500
429 air masses are advected western from the Atlantic Ocean. CT5 is similar to C1
430 (extratropical cyclone at the NW IP) described by García-Valero *et al.* (2012),
431 especially frequent in spring.

CT6 is the least frequent CT (10%) and occurs in winter, especially in January. In CT6 the Azores high (~1024 hPa) is located over the Canary Islands and southeastern IP (Fig. 5f) and the Icelandic low is located between the British Isles and Iceland with high intensity (984 hPa). Between both action centres a significant horizontal pressure gradient over Western Europe is established. There is zonal advection from the Western Atlantic affecting Western Europe and northern IP. The geopotential height field structure at 500 hPa is similar to that at the surface. When the pressure gradient dissipates CT6 is usually replaced by CT4. Nevertheless, when the Icelandic low is in a southern location CT6 is replaced by CT5, characterized by W-NW advection. CT6 has been identified by García-Valero *et al*. (2012) as an extratropical cyclone close to the British Isles with zonal flow aloft over the IP (Z1). Unlike CT6 only the western and central IP are affected by Atlantic advection in CT5.

Concerning the persistence, the mean persistence for all CTs is 3 days. A similar result (3.4 days) was obtained by Cahynová and Huth (2009) when performing an automatic synoptic classification over a similar spatial domain (IP and Western Mediterranean 17W/9E – 31N/48N) and temporal range (1957-2002) using ERA-40 reanalysis database and a k-means cluster technique. The maximum persistence is 27 days (CT4) and several episodes of 23 consecutive days occur in summer (CT1 and CT2).

3.3 Temporal stability of the classification and yearly classification

Results of temporal stability range from 34% for the year 1988 to 68% for the year 2012 with a mean of 51% for the 30 years (Fig. 6a). There is not a clear trend in the temporal stability over the period. Consecutive years can rank similar (1998-1999, 57% to 56%) or very different (1988-1989, 34% to 55%) total stability. The heterogeneity of the results indicates the inter-annual variability of synoptic circulation over the area.

456 The year 2012 stands out as the most similar to the climatic period which makes it especially useful to characterize CTs based on the data for that year only. Comparisons of the climatic CTs with 2012 CTs depict that overall, the position of the action centres and the spatial structure of the pressure fields (mslp and Z500) are equivalent to those discussed for the climatic period. The main differences between climatic and 2012 CTs are found in CT1 and CT5. In CT1, there is NW surface advection over the 1983-2012 period whereas it is N in 2012 (Fig. 5g) most likely caused by the latitude of the Azores high being 10º higher (50ºN) than in the climatic period (40ºN). Regarding CT5 (Fig. 5k), the low pressure system over the British Isles is deeper in the climatic period (994 hPa) than in 2012 (1000 hPa), which establishes NW advection in 2012 and W over 1983-2012.

467 CT1 and CT2 are the most frequent CTs in both periods (Table 2). CT4 and CT5 are two times more frequent during 2012 than in the climatic period, whereas CT3 is rarer in 2012. The least frequent climatic CT (CT6) has a similar frequency compared with 2012. The period of the year in which each CT is more frequent is alike for both classifications except for CT3. Whereas in the climatic period this anticyclonic CT is equally present in all months, it only appears in winter and the beginning of spring in 2012.

474 During 2012 the mean persistence for the six CTs is 3.5 days (0.5 days higher than the climatic mean) nevertheless there is a prominence of short-lived (1-day) CTs. The maximum persistence in 2012 is lower than the one found in 1983-2012.

477 Considering the temporal stability by CT derived for 2012 (Fig. 6b), the most stable is CT4 with 91% of the data evenly classified, followed by CT6, CT2 and CT5 with 79%,

73% and 70%, respectively. CT3 is the least stable of all the CTs with only half of the 2012 days classified in the same CT as in 1983-2012.

This characterization has also been performed for the 2nd and 3rd most stable years (1990 and 1995 respectively), showing similar results as those of 2012. The characteristics of the identified CTs and their associated pressure maps are provided as supplementary material (S4).

3.4 Identification of representative days

The representative day of each CT minimizes the Representative Day Score, a score that computes the distance from the daily grid to the average CT grid. On representative days the surface pressure and Z500 situations depicted on 2012 CTs maps (Fig. 5m to 5r) are accurately reproduced.

3.5 HYSPLIT back-trajectories on representative days

For 2012 representative days, back-trajectories ending at the cities cited in Fig. 2a are obtained by means of the HYSPLIT model (Fig. 7 for single back-trajectories and Supplementary Material – S5, for ensemble back-trajectories). Back-trajectories at 1500 magl for July 29th (CT1) show a NW origin in Santiago de Compostela, Bilbao, and Seville whereas in Madrid, Zaragoza, Barcelona and Palma the Mallorca the advection is from the W or SW. At 5500 magl back-trajectories mainly show a NW origin, confirming the maritime polar advection identified by the synoptic classification (ensemble back-trajectories are homogenous both at surface and Z500).

On August 19th (CT2) there is a dominance of S winds at 1500 magl over the inland IP, as well as in the Cantabrian coast. Although in the Mediterranean coast (Palma de Mallorca) the advection is mainly from the E. At 5500 magl there is a net transport of air masses from Morocco towards the IP derived from the presence of a high pressure system over the Northwestern Mediterranean Basin. Except for Santiago de Compostela, 5500 magl back-trajectories and their ensembles show African advection which is consistent with the synoptic pattern characterized by CT2.

On May 24th (CT3) 1500 magl back-trajectories in the eastern IP have a N-NE origin, coming mainly from France as shown in the ensemble back-trajectories at Barcelona, Bilbao and Zaragoza (Figure 7). Nevertheless, the continental advection from the NE is not clearly depicted in the southern and western IP. Similarly at 5500 magl, back-trajectories are from the N-NE in the northeastern IP and the Balearic Islands (Bilbao, Zaragoza, Barcelona and Palma).

Polar maritime advection that characterizes CT4 is confirmed by the back-trajectories, both single and ensemble, on January 24th that show a N-NW origin for all the considered cities both at 1500 and 5500 magl.

In the western and central IP, 1500 magl back-trajectories on October 16th (CT5) have an Atlantic origin (W/NW). However, in the Spanish Mediterranean coast (Barcelona and Palma) the advection is from the S-SE. At 5500 magl all of the back-trajectories depict Atlantic maritime advection (ensembles are homogenous). There is an anticyclone over Italy that establishes S winds in the Spanish Mediterranean coast.

Zonal Atlantic advection, characteristic of CT6, is clearly depicted in the single and ensemble back-trajectories of its representative day (January 1st), both at 1500 and 5500 magl for all the considered cities. Contrary to CT5, at 1500 magl the strong westerlies are not obstructed by topographic barriers affecting the atmospheric dynamics in the Spanish Mediterranean coast.

Overall, the obtained results of single and ensemble back-trajectories are consistent with the origin of the air masses depicted in the CTs. Path and speed of the air masses as calculated by the HYSPLIT model confirm that the synoptic circulation is in agreement with the one described in each CT both at 1500 and 5500 magl.

3.6 NO_2 concentration dynamics on CT representative days over the IP

For the characterization of NO_2 dynamics, 1h-maximum NO_2 concentration maps from the CALIOPE-AQFS (Fig. 8) have been analysed for the representative days of 2012. Special focus is over five areas within the IP (Fig. 2b) that frequently show high NO_2 concentrations (1h-maximum > 40 $\mu g\, m^{-3}$. They are the two biggest cities of Spain (Madrid and Barcelona > 5 million inhabitants), the urban-industrial area of Valencia (1.5 million inhabitants), the industrial area of Algeciras (there are two power plants, a refinery and it is a hotspot of maritime traffic), and the energy generation area of Asturias (there are five power plants and three cocking plants).

On July 29th, 2012 (Fig. 8, CT1), northwesterlies in the Cantabrian coast reach 10-15 $m\, s^{-1}$ and transport NO_2 emissions from Asturias towards the S (40 $\mu g\, m^{-3}$ at 40 km) till the Cantabrian mountains (2000 masl). Synoptic northerlies follow the Portuguese coastline reaching the Gulf of Cadiz and become westerlies in Algeciras (10-15 $m\, s^{-1}$) transporting the NO_2 plume towards the E (40 $\mu g\, m^{-3}$ at 115 km) during the morning; then the wind becomes weak enabling the transport of locally emitted NO_2 through sea breeze till 30 km to the NW (60 $\mu g\, m^{-3}$). The Guadarrama mountains (2200-2400 masl), with a NE-SW orientation north of the metropolitan area of Madrid, prevent the arrival of N-NW winds (~5 $m\, s^{-1}$) towards the capital, leading to more stagnant atmospheric conditions; thus, Madrid urban plume remains within the metropolitan area (~20 km, 80 $\mu g\, m^{-3}$). Northern synoptic winds, channelled between the Pyrenees and the French

Central Massif favour the establishment of an anticyclonic atmospheric circulation in the area of Barcelona that transport NO_2 towards the S during dawn (50 µg m^{-3} at 40 km) and to the SW, parallel to the coast (~40 km) during the morning reaching 30 µg m^{-3}; in the afternoon southern winds towards Barcelona transport the plume to the N (30 µg m^{-3} at 30 km). In Valencia, the development of mesoscale processes control NO_2 transport; sea breezes penetrate inland through the Jucar Valley.

August 19th, 2012 is characterised by a reduced surface pressure gradient over Western Europe (Fig. 8, CT2) that enables a mesoscale control of surface dynamics. The plume in Asturias is transported without a dominant direction. NO_2 emissions from Algeciras are mainly transported by easterlies towards the Gulf of Cadiz reaching 40 µg m^{-3} at 100 km; meanwhile in the evening there is a short-distance transport to the NW from the area of emissions (60 µg m^{-3} at 20 km). Madrid's urban plume remains stationary with a maximum displacement of 20 km (southern winds ~5 m s^{-1}, 80 µg m^{-3}). Along the Mediterranean coast, NO_2 dynamics are dominated by land-sea breezes that drive plumes on a daily cycle: towards the sea at night, inland at noon and perpendicular to the coast in the morning and the afternoon.

Under a blocking anticyclone over the North Sea, E-NE advection is established towards the IP (Fig. 8, CT3), as observed in May 24th, 2012. NE winds in the Cantabrian coast (~15 m s^{-1}) transport Asturias NO_2 towards the W (30 µg m^{-3} at 50 km). In Algeciras, strong E winds favour NO_2 transport (40 µg m^{-3}) towards the Gulf of Cadiz (~150 km). In the urban area of Madrid, the synoptic E-NE winds are channelled through the Tajo Valley (NE-SW orientation) leading to a SW transport of the urban plume (40 µg m^{-3}, 40 km). Strong northerlies (~25 m s^{-1}) are channelled through the Rhone Valley favouring an anticyclonic circulation over the Balearic Islands that lead to a transport of Barcelona's plume in an E direction during the morning (40 km) and N-NE in the afternoon (30 km). In Valencia, synoptic winds arrive from the E leading to a net transport of the plume (~30 µg m^{-3} at 30 km) towards the NW through the Turia Valley, and the W through the Jucar Valley.

On January 24th, 2012 (Fig. 8, CT4) northerlies (~10 m s^{-1}) arriving to the northern IP shift into easterlies when they reach the coast, transporting NO_2 from Asturias (40 µg m^{-3}) towards the W reaching 40 km. In Algeciras, transport is dominated by westerlies during the morning (40 µg m^{-3} are reached till 120 km); in the afternoon, the strengthening of a low pressure system located S of the Gulf of Cadiz initiates a change of dominant wind direction, enhancing easterlies to transport Algeciras's plume (40 µg m^{-3}) 100 km to the W. In the Madrid area, northerlies (~5 m s^{-1}) are channelled through the Tajo Valley transporting the NO_2 urban plume towards the SW; nevertheless, wind speed is higher in CT4 than in CT3 and the urban plume goes further, reaching the same concentration (40 µg m^{-3}) at 70 km. N-NW synoptic winds are channelled between the Pyrenees and the French Central Massif, establishing N winds towards the NW IP (15 m s^{-1}), transporting Barcelona's urban plume (40 µg m^{-3}) to the S-SE (100 km) during the morning; in contrast, in the evening and at night, NO_2 (40 µg m^{-3}) is transported to the NE parallel to the coast and forced by the Pre-coastal mountain range reaching 85 km away from Barcelona. With CT4, surface westerly winds are weakened as they pass through the IP, leading to mesoscale control of NO_2 transport over Valencia; during the night, land-breezes transport NO_2 towards the sea up to 20 km (40 µg m^{-3}), whereas during the day, the urban plume is transported by sea-breezes towards the NW, channelled by the Turia Valley, up to 40 km.

Under the W-NW advective CT5, on October 16th, 2012 (Fig. 8, CT5), southwesterlies and westerlies reach up to 15 m s^{-1} and transport Asturias' plume to the NE (10 µg m^{-3}, 50 km). In the southern IP there is a short-range (20 km) transport of NO_2 towards the SE of the Algeciras Bay (80 µg m^{-3}) in the morning, followed by short-range W transport at noon (40 µg m^{-3} at 20 km). Westerlies arriving to Madrid (10-15 m s^{-1}) during the night transport the urban plume (30 µg m^{-3}) towards the E-NE up to 60 km; in the afternoon Madrid's NO_2 urban plume (50 µg m^{-3}) is channelled through the Henares and Jalon Valleys (NE orientation) and transported 80 km away. The Spanish Mediterranean coast is less affected by the synoptic W-NW advection because winds are weakened by topographic barriers (Iberian System, Baetic System, Catalan mountain range) on their way to the east. Thus, Barcelona's urban plume is mainly controlled by land-sea breezes; NO_2 is transported towards the NE parallel to the Pre-coastal mountain range during the day (30 µg m^{-3} at 50 km). In Valencia, the transport of NO_2 is dominated by easterlies and channelled by the Jucar Valley (40 µg m^{-3} at 30 km).

Atlantic zonal winds arriving to the IP (Fig. 8, CT6), are present on January 1st, 2012. Strong westerlies (30 m s^{-1}) arrive to the Cantabrian coast transporting Asturias' plume towards the E-NE, reaching up to 100 km at dawn (10 µg m^{-3}). In Algeciras, westerlies transport the NO_2 plume to the E reaching the Alboran Sea (200 km, 30 µg m^{-3}). Madrid's urban plume (40 µg m^{-3}) is channelled in a NE direction through the Henares and Jalon Valleys up to 150 km, especially in the evening. Western synoptic winds are strong enough to overcome the topographical barriers and reach the Mediterranean coast. In Barcelona and Valencia areas, westerlies transport NO_2 towards the Mediterranean Sea (40 µg m^{-3} at 90 and 60 km away, respectively); nevertheless, in the afternoon, westerlies become weak leading to short-distance dispersion without a dominant direction.

Locally high NO_2 concentrations are observed in Asturias under CT1, CT2 and CT4; during these CTs the plume is transported at short distance associated to weaker winds compared to those in CT3, CT5, and CT6 when there is a dominance of stronger winds that enhance the dispersion of NO_2. In the Algeciras area, the transport is mainly controlled by easterlies (CT2, CT3, and CT4) and westerlies (CT1, CT5, and CT6) derived from synoptic circulation; nevertheless, for the most frequent patterns when there is a shift in wind direction the local transport towards the NW leads to high NO_2 concentration in the Algeciras area. In the central IP synoptic circulation, together with the Guadarrama mountains, control NO_2 transport; towards the SW channelled by the Tajo Valley during CT3 and CT4 or less frequently towards the NE channelled through the Henares and Jalon Valleys under CT5 and CT6. The progression of Atlantic synoptic air masses is weakened in their way towards the Spanish Mediterranean coast in four CTs (69% of climatic frequency), enabling mesoscale recirculation of NO_2 (driven by land-sea and mountain-valley breezes), perpendicular to the coast along the Barcelona and Valencia areas. Only under the influence of E-NE advection (CT3, 21% of climatic frequency) and Western Atlantic zonal advection (CT6, 10%), synoptic circulations control NO_2 transport along the Mediterranean coast.

Complementary, modelled daily NO_2 concentrations from CALIOPE-AQFS at air quality stations belonging to the Spanish air quality monitoring network over the previously discussed five areas have been boxplotted per CT, using daily data of year 2012 (Fig. 9). Overall, CT2 that is characterised by a reduced surface pressure gradient presents the highest mean NO_2 concentration. Despite being a typical summertime pattern when NO_2 emissions are at its annual minimum (Guevara *et al.*, 2013), the lack of surface advection favours the accumulation of NO_2 during consecutive days, enhancing high NO_2 concentrations. On the other hand CT6, which is the most infrequent pattern, shows the second highest NO_2 concentrations of all the CTs, in the Mediterranean coastal areas and Madrid. In Madrid, these concentration records are probably related with a low planetary boundary layer height (300 masl at 12:00 UTC, as forecasted by the WRF-ARW model, compared to ~600 masl for CT4; 1500 masl for CT3 and CT5; and 1800 masl for CT1 and CT2).

4 Conclusions

The present work has established an objective procedure to establish a circulation type classification on a climatic basis (1983-2012) to characterize air quality dynamics over the IP. Considering that there is not a single synoptic classification that best fits for all purposes (Huth *et al.*, 2008), sensitivity analyses to several classification techniques and factors affecting it have been performed in order to objectivize the set-up that maximizes its quality. Automatic classification techniques based on k-means clustering perform better in terms of EV than correlation-based and PCA-based techniques. Within the k-mean techniques, CKM guarantees the identification of non-extreme CTs, with maximum separability and minimum within-type variability using a reasonable amount of computing resources. The classification quality increases with the number of CTs, although this relation is not linear. A 5% increase threshold in EV is established in order to settle an appropriate number of CTs leading to a selection of six CTs. Surface pressure is the reference proxy variable chosen because it obtains the best EV (among the non-seasonalised variables) and informs about the stability/instability of the atmosphere and the wind speed and direction, which helps understanding air quality dynamics. Although surface level depicts lower EV than higher vertical levels (below 700 hPa), the surface is selected in the reference set-up because most of the processes involved in air quality occur within the lower levels of the atmosphere. The domain size is a critical factor when performing synoptic classifications because the identified CTs for each domain have different spatial, temporal, and dynamic characteristics. The medium-sized domain (D01) is selected in the reference set-up because it covers areas that are the origin of the air masses towards the IP while ranking an average EV (0.48).

The three most common CTs account for 67.6% of climatic frequency (CT1, CT2, and CT3) and mainly occur in summertime, replacing one another. While CT1 (23.9%) is a NW advective pattern characterized by the arrival of polar maritime air masses towards the IP determined by the presence of the Azores high, CT2 (22.4%) depicts a reduced pressure surface gradient, enabling the development of the Iberian thermal low; although stagnant conditions dominate at the surface in CT2, there is a net advection of North African air masses at Z500. Despite being present throughout the year, CT3 (21%) is especially frequent in spring and summer as a result of a blocking anticyclone over central Europe that leads to E-NE advection towards the IP. When the high pressure system subsides, CT3 tends to be replaced by CT2. In winter two CTs are especially frequent, CT4 (12%) and CT6 (10%). The former is an anticyclonic situation that enables the arrival of Atlantic air masses towards the IP, whereas the latter is characterised by zonal Atlantic maritime advection. Finally, CT5 (10%) presents unstable conditions over the IP with W-NW winds and precipitation, and it is typical of transitional seasons. Topographic barriers in the central and eastern IP (Iberic System, Baetic System, Catalan mountain range) are overcome by westerlies on their way to the Spanish Mediterranean coast in CT6 but not in CT5.

Although inter-annual variability exists, the classification is temporally stable showing consistent CTs when using yearly data. The year 2012 is the representative year of this climatic period because its CTs show the highest temporal stability (67.8%). The CTs obtained with the reference set-up for the climatic period and 2012 are consistent with synoptic patterns over the IP found in the literature (Martín-Vide and Olcina, 2001, García-Valero *et al*., 2012, Fig. 2b). A representative day of 2012 for each CT has been objectively identified by means of the Representative Day Score. Single and ensemble Back-trajectories obtained with the HYSPLIT model confirm the synoptic flows depicted by each CT on representative days.

The analysis of NO_2 concentration maps over the IP associated with the six CTs in 2012 shows that synoptic circulation contributes to explain the spatial distribution of urban and industrial NO_2 plumes. Synoptic circulation influences the intensity of the advection and the planetary boundary layer height favouring or limiting the air pollutant dispersion. Regarding the influence of the CT on NO_2 transport, two main regions within the IP are distinguished: 1) areas of central, northern, and southern IP where there is a synoptic control of NO_2 under all of the CTs; and 2) Mediterranean coastal areas, where in 4 CTs (69% of climatic frequency) synoptic forcing is weakened, and a combined approach of synoptic and mesoscale dynamics control the NO_2 concentrations. Explaining the spatiotemporal dynamics of air pollution patterns under typical circulation types is useful to properly develop air quality plans and atmospheric pollution risk assessments.

Acknowledgements

The ECMWF is acknowledged for the provision of ERA-Interim data. The COST733 is also thanked for the software. All simulations were performed on the MareNostrum supercomputer hosted by the Barcelona Supercomputing Center. This work is partially funded by the Iberdrola Foundation by means the pre-doctoral grant held by V. Valverde, the post-doctoral grant held by M.T. Pay in the Beatriu de Pinós programme (2011 BP-A 00427), and the Severo Ochoa Program awarded by the Spanish Government (SEV-2011-00067). The authors declare that there are no conflicts of interest.

References

Alonso-Pérez S, Cuevas E, Querol X. 2011. Objective identification of synoptic meteorological patterns favouring African dust intrusions into the marine boundary layer of the subtropical eastern north Atlantic region. *Meteorology and Atmospheric Physics* **113:** 109–124. DOI: 10.1007/s00703-011-0150-z.

Azorin-Molina C, Chen D, Tijm S, Baldi M. 2009. A multi-year study of sea breezes in a Mediterranean coastal site: Alicante (Spain). *International Journal of Climatology*. DOI: 10.1002/joc.2064.

Baldasano JM, Cremades L, Soriano C. 1994. Circulation of Air Pollutants over the Barcelona Geographical Area in Summer. Proceedings of Sixth European Symposium Physico-Chemical Behaviour of Atmospheric Pollutants. Varese (Italy), 18-22 October, 1993. Report EUR 15609/1 EN: 474-479.

Baldasano JM, Jiménez-Guerrero P, Jorba O, Pérez C, López E, Güereca P, Martin F, García-Vivanco M, Palomino I, Querol X, Pandolfi M, Sanz MJ, Diéguez JJ. 2008. CALIOPE: An operational air quality forecasting system for the Iberian Peninsula, Balearic Islands and Canary Islands. First annual evaluation and ongoing developments. *Advances in Science and Research* **2:** 89-98. DOI: 10.5194/asr-2-89-2008.

Baldasano JM, Pay MT, Jorba O, Gassó S, Jiménez-Guerrero P. 2011. An annual assessment of air quality with the CALIOPE modeling system over Spain. *Science of the Total Environment* **409:** 2163-2178. DOI: 10.1016/j.scitotenv.2011.01.041.

Barros N, Toll I, Soriano C, Jiménez P, Borrego C, Baldasano JM. 2003. Urban Photochemical Pollution in the Iberian Peninsula: Lisbon and Barcelona Airsheds.

744 *Journal of the Air & Waste Management Association* **53:** 347-359. DOI: 10.1080/10473289.2003.10466157.

746 Basart S, Pérez C, Nickovic S, Cuevas E, Baldasano JM. 2012. Development and evaluation of the BSC-DREAM8b dust regional model over Northern Africa, the Mediterranean and the Middle East. *Tellus Series B – Chemical and Physical Meteorology* **64:** 1-12. DOI: 10.3402/tellusb.v64i0.18539.

750 Beck C, Philipp A. 2010. Evaluation and comparison of circulation type classifications for the European domain. *Physics and Chemistry of the Earth, Parts A/B/C* **35:** 374-387. DOI: 10.1016/j.pce.2010.01.001.

753 Beck C, Philipp A, Streicher F. 2013. The effect of domain size on the relationship between circulation type classifications and surface climate. *International Journal of Climatology*. DOI: 10.1002/joc.3860.

756 Byun DW, Schere KL. 2006. Review of the governing equations, computational algorithms and other components of the Models-3 Community Multiscale Air Quality (CMAQ) Modeling System. *Applied Mechanics Reviews* **59:** 51-77. DOI: 10.1115/1.2128636.

760 Cahynová M, Huth R. 2009. Enhanced lifetime of atmospheric circulation types over Europe: fact or fiction? *Tellus* **61A:** 407-416. DOI: 10.1111/j.1600-0870.2009.00393.x.

762 CALIOPE Air Quality Forecasting System website: www.bsc.es/caliope

763 Casado MJ, Pastor MA, Doblas-Reyes FJ. 2010. Links between circulation types and precipitation over Spain. *Physics and Chemistry of the Earth* **35:** 437-447. DOI: 10.1016/j.pce.2009.12.007.

Casado MJ, Pastor MA. 2013. Circulation types and winter precipitation in Spain. *International Journal of Climatology*. DOI: 10.1002/joc.3860.

Cassou C, Terray L, Phillips A. 2005. Tropical Atlantic influence on European heat waves. *Journal of Climate* **18:** 2805-2811. DOI: 10.1175/JCLI3506.1.

Castell-Balaguer N, Téllez L, Mantilla E. 2012. Daily, seasonal and monthly variations in ozone levels recorded at the Turia river basin in Valencia (Eastern Spain). *Environmental Science and Pollution Research* **19:** 3461-3480. DOI: 10.1007/s11356-012-0881-5.

Dee DP, Uppala SM, Simmons AJ, Berrisford P, Poli P, Kobayashi S, Andrae U, Balmaseda MA, Balsamo G, Bauer P, Bechtold P, Beljaars ACM, van de Berg L, Bidlot J, Bormann N, Delsol C, Dragani R, Fuentes M, Geer AJ, Haimberger L, Healy SB, Hersbach H, Hólm EV, Isaksen L, Kållberg P, Köhler M, Matricardi M, McNally AP, Monge-Sanz BM, Morcrette JJ, Park BK, Peubey C, de Rosnay P, Tavolato C, Thépaut JN, Vitart F. 2011. The ERA-Interim reanalysis: configuration and performance of the data assimilation system. *Quarterly Journal of the Royal Meteorological Society* **137:** 553-597. DOI: 10.1002/qj.828.

Demuzere M, Trigo RM, Vila-Guerau de Arellano J, van Lipzig NPN. 2009. The impact of weather and atmospheric circulation on O_3 and PM10 levels at a rural mid-latitude site. *Atmospheric Chemistry and Physics* **9:** 2695-2714. DOI: 10.5194/acp-9-2695-2009.

Demuzere M, Kassomenos P, Philipp A. 2011. The COST733 circulation type classification software: an example for surface ozone concentrations in Central Europe. *Theoretical and Applied Climatology* **105:** 143-166. DOI: 10.1007/s00704-010-0378-4.

Draxler RR, Rolph GD. 2013. HYSPLIT (HYbrid Single-Particle Lagrangian Integrated Trajectory) Model access via NOAA ARL READY Website (http://www.arl.noaa.gov/HYSPLIT.php). NOAA Air Resources Laboratory, College Park, MD.

Elminir HK. 2005. Dependence of urban air pollutants on meteorology. *Science of the Total Environment* **350:** 225-237. DOI: 10.1016/j.scitotenv.2005.01.043.

Erpicum M, Mabille G, Fettweis X. 2008. Automatic synoptic weather circulation types classification based on the 850 hPa geopotential height. In: Book of Abstracts COST 733 Mid-term Conference, Advances in Weather and Circulation Type Classifications & Applications, 22–25 October 2008 Krakow, Poland. 33 p.

Esteban P, Jones PD, Martín-Vide J, Moses M. 2005. Atmospheric circulation patterns related to heavy snowfall in Andorra, Pyrenees. *International Journal of Climatology* **25:** 319-329. DOI: 10.1002/joc.1103.

European Centre for Medium-Range Weather Forecast ERA-Interim reanalysis webserver: http://apps.ecmwf.int/datasets/data/interim_full_daily/

Fereday D, Knight J, Scaife A, Folland C. 2008. Cluster analysis of North Atlantic-European circulation types and links with tropical Pacific Sea surface temperatures. *Journal of Climate* **21:** 3687-3703. DOI: 0.1175/2007JCLI1875.1.

Flocas H, Kelessis A, Helmis C, Petrakakis M, Zoumakis M, Pappas K. 2009. Synoptic and local scale atmospheric circulation associated with air pollution episodes in an urban Mediterranean area. *Theoretical and Applied Climatology* **95:** 265-277. DOI: 10.1007/s00704-008-0005-9.

Ganor E, Osentinsky I, Stupp A, Alpert P. 2010. Increasing trend of African dust, over 49 years, in the eastern Mediterranean. *Journal of Geophysical Research* **115:** D07201. DOI: 10.1029/2009JD012500.

García-Bustamante E, González-Rouco J, Navarro J, Xoplaki E, Jiménez P, Montávez J. 2012. North Atlantic atmospheric circulation and surface wind in the northeast of the Iberian Peninsula: uncertainty and long term downscaled variability. *Climate Dynamics* **38:** 141-160. DOI: 10.1007/s00382-010-0969-x.

García-Valero JA, Montávez JP, Jérez S, Gómez-Navarro JJ, Lorente-Plazas R, Jiménez-Guerrero P. 2012. A seasonal study of the atmospheric dynamics over the Iberian Peninsula based on circulation types. *Theoretical and Applied Climatology* **110:** 219-310. DOI: 10.1007/s00704-012-0623-0.

Giorgi F, Meleux F. 2007. Modelling the regional effects of climate change on air quality. *Comptes Rendus Geoscience* **339:** 721-733. DOI: 10.1016/j.crte.2007.08.006.

Gonçalves M, Jiménez-Guerrero P, Baldasano JM. 2009. Contribution of atmospheric processes affecting the dynamics of air pollution in South-Western Europe during a typical summertime photochemical episode. *Atmospheric Chemistry and Physics* **9:** 849-864. DOI: 10.5194/acp-9-849-2009.

Guevara M, Martínez F, Arévalo G, Gassó S, Baldasano JM. 2013. An improved system for modelling Spanish emissions: HERMESv2.0. *Atmospheric Environment* **81:** 209-221. DOI: 10.1016/j.atmosenv.2013.08.053.

Huth R, Beck C, Philipp A, Demuzere M, Ustrnul Z, Cahynová M, Kyselý J, Tveito OE. 2008. Classifications of atmospheric circulation patterns: recent advances and applications. *Annals of the New York Academy of Science* **1146:** 105-152. DOI: 10.1196/annals.1446.019.

James P. 2007. An objective classification method for Hess and Brezowsky Grosswetterlagen over Europe. *Theoretical and Applied Climatology* **88:** 17-42. DOI: 10.1007/s00704-006-0239-3.

Jiménez PA, González-Rouco JF, Montávez JP, García-Bustamante E, Navarro J. 2009. Climatology of wind patterns in the northeast of the Iberian Peninsula. *International Journal of Climatology* **29:** 501-525. DOI: 10.1002/joc.1705.

Kirchhofer W. 1974. Classification of European 500 mb patterns. Working Reports of the Swiss Meteorological Institute. Zürich. 16 p.

Kruizinga S. 1979. *Objective classification of daily 500 mbar patterns*. In: Preprints Sixth Conference on Probability and Statistics in Atmospheric Sciences, Banff, Alberta. American Meteorological Society, Boston, MA.

Martín-Vide J, Olcina J. 2001. *Climas y tiempos de España*. Alianza Editorial: Madrid, Spain.

Michelangeli P, Vautard R, Legras B. 1995. Weather regimes: recurrence and quasi stationarity. *Journal of the Atmospheric Sciences* **52:** 1237-1256. DOI: 10.1175/1520-0469(1995)052<1237:WRRAQS>2.0.CO;2.

Millán M, Artíñano B, Alonso L, Navazo M, Castro M. 1991. The effect of the mesoscale flows on regional and long-range atmospheric transport in western Mediterranean area. *Atmospheric Environment* **25A:** 949-963. DOI: 10.1016/0960-1686(91)90137-V.

Millán M, Salvador R, Mantilla E, Kallos G. 1997. Photooxidant dynamics in the Mediterranean basin in summer: results from European research projects. *Journal of Geophysical Research* **102:** 8811–8823. DOI: 10.1029/96JD03610.

Pay MT, Jiménez-Guerrero P, Baldasano JM. 2011. Implementation of resuspension from paved roads for the improvement of CALIOPE air quality system in Spain. *Atmospheric Environment* **45:** 802-807. DOI: 10.1016/j.atmosenv.2010.10.032.

Pay MT, Jiménez-Guerrero P, Jorba O, Basart S, Pandolfi M, Querol X, Baldasano JM. 2012. Spatio-temporal variability of levels and speciation of particulate matter across Spain in the CALIOPE modeling system. *Atmospheric Environment* **46:** 376-396. DOI: 10.1016/j.atmosenv.2011.09.049.

Pay MT, Martínez F, Guevara M, Baldasano JM. 2014. Air quality at kilometre scale grid over Spanish complex terrains. *Geoscientific Model Development Discussions* **7:** 2293-2334. DOI: 10.5194/gmdd-7-2293-2014.

Pérez C, Nickovic S, Baldasano JM, Sicard M, Rocadenbosch F, Cachorro VE. 2006a. A long Saharan dust event over the western Mediterranean: Lidar, Sun photometer observations, and regional dust modeling. *Journal of Geophysical Research* **111:** D15214. DOI: 10.1029/2005JD006579.

Pérez C, Nickovic S, Pejanovic G, Baldasano JM, Ozsoy E. 2006b. Interactive dust-radiation modeling: A step to improve weather forecasts. *Journal of Geophysical Research* **111:** D16206. DOI: 10.1029/2005JD006717.

875 Petisco E. 2003. *Metodología para una caracterización de la circulación atmosférica en el entorno de la Península Ibérica y Baleares*. Nota técnica n 9. Instituto Nacional de Meteorología.

878 Philipp A, Della-Marta PM, Jacobeit J, Fereday DR, Jones PD, Moberg A, Wanner H. 2007. Long-Term Variability of Daily North Atlantic–European Pressure Patterns since 1850 Classified by Simulated Annealing Clustering. *Journal of Climate* **20:** 4065-4095. DOI: 10.1175/JCLI4175.1.

882 Philipp A, Bartholy J, Beck C, Erpicum M, Esteban P, Fettweis X, Huth R, James P, Jourdain S, Kreienkamp F, Krennert T, Lykoudis S, Michalides S, Pianko K, Post P, Rasilla Álvarez D, Schiemann R, Spekat A, Tymvios FS. 2010. COST733CAT - a database of weather and circulation type classifications. *Physics and Chemistry of the Earth* **35:** 360-373. DOI: 10.1016/j.pce.2009.12.010.

887 Philipp A, Beck C, Huth, R, Jacobeit, J. 2014. Development and comparison of circulation type classifications using the COST 733 dataset and software. *International Journal of Climatology*. DOI: 10.1002/joc.3920.

890 Pineda N, Esteban P, Trapero L, Soler X, Beck C. 2010. Circulation types related to lightning activity over Catalonia and the Principality of Andorra. *Physics and Chemistry of the Earth* **35:** 469-476. DOI: 10.1016/j.pce.2009.12.009.

893 Rand WM. 1971. Objective criteria for the evaluation of clustering methods. *Journal of the American Statistical Association* **66:** 846-850. DOI: 10.1080/01621459.1971.10482356.

Rasilla D. 2003. Aplicación de un método de clasificación sinóptica a la Península Ibérica. *Investigaciones Geográficas* **30:** 27-45.

Romero R, Sumner G, Ramis C, Genovés A. 1999. A classification of the atmospheric circulation patterns producing significant daily rainfall in the Spanish Mediterranean area. *International Journal of Climatology* **19:** 765-785. DOI: 10.1002/(SICI)1097-0088(19990615)19:7<765::AID-JOC388>3.0.CO;2-T.

Russo A, Trigo RM, Martins H, Mendes MT. 2014. NO_2, PM10 and O_3 urban concentrations and its association with circulation weather types in Portugal. *Atmospheric Environment* **89:** 768-785. DOI: 10.1016/j.atmosenv.2014.02.010.

Saavedra S, Rodríguez A, Taboada JJ, Souto JA, Casares JJ. 2012. Synoptic patterns and air mass transport during ozone episodes in northwestern Iberia. *Science of the Total Environment* **441:** 97-110. DOI: 10.1016/j.scitotenv.2012.09.014.

Salvador P, Artíñano B, Querol X, Alastuey A. 2008. A combined analysis of backward trajectories and aerosol chemistry to characterise long-range transport episodes of particulate matter: The Madrid air basin, a case study. *Science of the Total Environment* **390:** 495-506. DOI: 10.1016/j.scitotenv.2007.10.052.

Salvador P, Artíñano B, Molero F, Viana M, Pey J, Alastuey A, Querol X. 2013. African dust contribution to ambient aerosol levels across central Spain: Characterization of long-range transport episodes of desert dust. *Atmospheric Research* **127:** 117-129. DOI: 10.1016/j.atmosres.2011.12.011.

Seinfeld JH, Pandis SN. 2006. *Atmospheric Chemistry and Physics: From Air Pollution to Climate Change*. John Wiley & Sons, Inc: New York, USA.

Skamarock WC, Klemp JB. 2008. A time-split nonhydrostatic atmospheric model for weather research and forecasting applications. *Journal of Computational Physics* **227:** 3465-3485. DOI: 10.1016/j.jcp.2007.01.037.

Shrestha KL, Kondo A, Kaga A, Inoue Y. 2009. High-resolution modelling and evaluation of ozone air quality of Osaka using MM5-CMAQ system. *Journal of Environmental Science* **21:** 782-789. DOI: 10.1016/S1001-0742(08)62341-4.

Yiou P, Nogaj M. 2004. Extreme climatic events and weather regimes over the North Atlantic: when and where? *Geophysical Research Letters* **31:** 1-4. DOI: 10.1029/2003GL019119.

Yiou P, Goubanova K, Nogaj M. 2008. Weather regime dependence of extreme value statistics for summer temperature and precipitation. *Nonlinear Processes in Geophysics* **15:** 365–378. DOI: 10.5194/npg-15-365-2008.

Zhang Y, Mao H, Ding A, Zhou D, Fu C. 2013. Impact of synoptic weather patterns on spatio-temporal variation in surface O_3 levels in Hong Kong during 1999-2011. *Atmospheric Environment* **73:** 41-50. DOI: 10.1016/j.atmosenv.2013.02.047.

Table 1: Characteristics of sensitivity tests performed for the climatic period, 1983-2012. Elements between commas indicate the tested variable in each case study.

# test	Studied factor	Variability range
1	Classification technique (clt)	1) Correlation techniques LND: Lund overall correlation coefficient KIR: Kirchofer partial correlation for each lat/lon ERP: Erpicum similarity index based on geopotential direction 2) Principal Component Analysis (PCA) PCT: obliquely rotated t-mode PCA PTT: orthogonally rotated t-mode PCA PXE: s-mode PCA with VARIMAX rotation PXK: t-mode PCA followed by a k-means cluster analysis 3) Clustering techniques HCL: hierarchical cluster KMN: k-means. Random seeds. DKM: Dk-means. Most dissimilar seeds. CKM: Ck-means. Most dissimilar seeds. 5% minimum frequency of each cluster. SAN: Simulated Annealing and Normalization
2	Number of circulation types (nCT)	From 2 to 15, 18, 27, 50
3	Meteorological variable used as proxy (iv)	Mean sea level pressure (mslp), 10-meter U and V wind components (UV10), 1000-hPa vorticity (Vort1000), 2-meter temperature (T2m), relative humidity (RH)
4	Vertical level (vl)	Surface, 11 geopotential levels from 1000 to 1 hPa each 100 hPa
5	Temporal resolution (tr)	Data each 6, 12, 24 hours, 06 h mean

6	Seasonality (se)	Winter, spring, summer, autumn, annual (an)
7	Horizontal resolution (hr)	0.125º x 0.125º, 0.25º x 0.25º, 0.75º x 0.75º, 1.5º x 1.5º, 3º x 3º
8	Spatial domain (d)	D00 (18.75N – 76.5N / 33.75W – 31.5 E), D01 (24.75N – 62.25N / 25.5W – 20.25 E), D02 (30N – 50.25N / 13.5W – 13.5 E)

Table 2: Characteristics of derived circulation types with the reference set-up (section 3.1) for the climatic period (1983-2012) and reference year 2012.

		CT1	CT2	CT3	CT4	CT5	CT6
Description		NW advection	Summer reduced surface pressure gradient	E/NE advection	Atlantic high with polar maritime advection	W/NW advection	Western Atlantic zonal advection
Criteria	Period						
Frequency (%)	1983-2012	23.9	22.4	21.3	12.0	10.4	10.1
	2012	21.9	21.6	8.8	17.8	20.5	9.3
Most frequent month	1983-2012	JUL	AUG	MAY	JAN	APR/OCT	JAN
	2012	JUL	AUG	FEB	JAN	APR/NOV	DEC
Seasonal frequency (%): DJF/ MAM/ JJA/ SON	1983-2012	10.1/26.1/ 43.5/ 20.3	11.7/26.2/ 35.8/ 26.3	25.9/28.5/ 23.5/22.0	49.8/19.9/ 4.4/25.9	26.0/28.7/ 10.4/35.0	54.3/16.4/ 1.9/27.4
	2012	2.5/37.5/ 37.5/22.5	15.2/20.3/ 43.0/21.5	56.3/43.8/ 0.0/ 0.0	56.9/21.5/ 6.2/15.4	5.3/21.3/ 29.3/44.0	50.0/5.9/ 5.9/38.2
Mean / Max persistence (days)	1983-2012	2.9 / 23	2.9 / 22	3.8 / 19	2.7 / 27	3.0 / 17	2.9 / 19
	2012	3.6 / 10	2.6 / 8	4.6 /18	3.8 /15	3.0 /10	3.5 / 10
Transitions	1983-2012	CT2	CT1	CT2	CT6	CT1	CT4
	2012	CT2/CT5	CT1/CT5	CT4	CT2	CT1/CT2	CT5

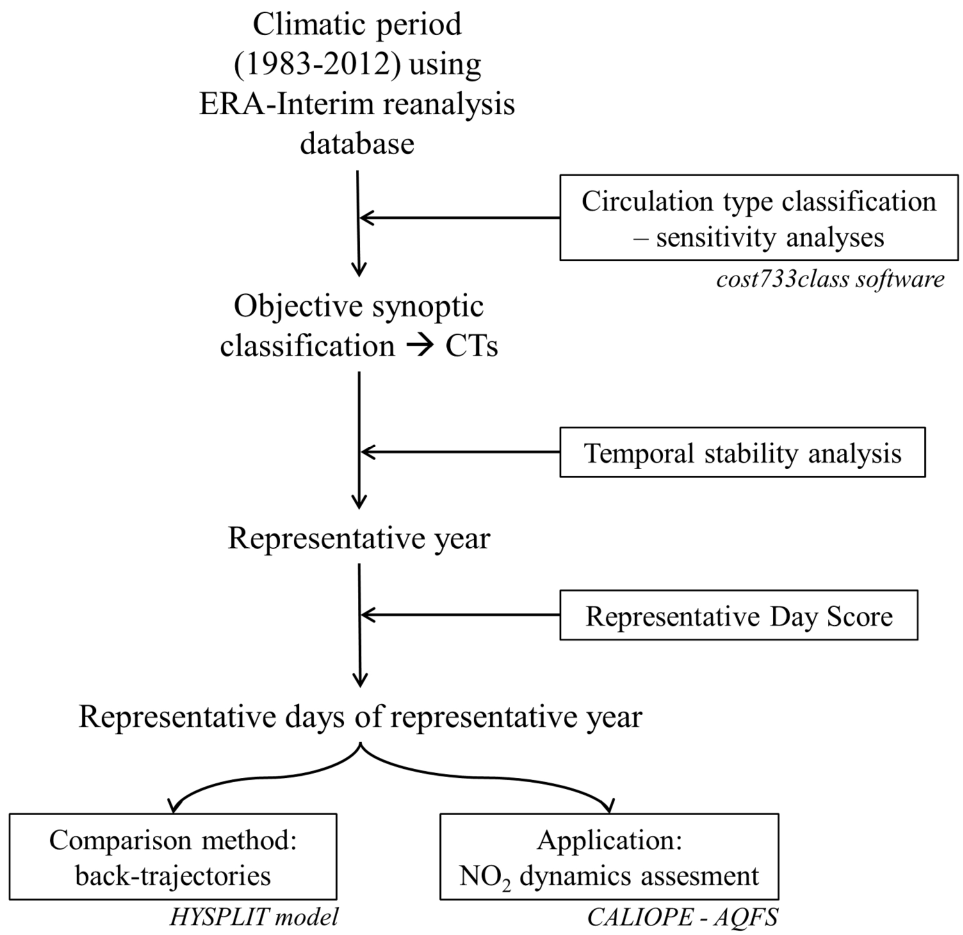

Figure 1. Methodological flowchart to obtain representative days of the objective circulation type classification. Methodologies are shown in boxes and tools are indicated in italics.
609x606mm (96 x 96 DPI)

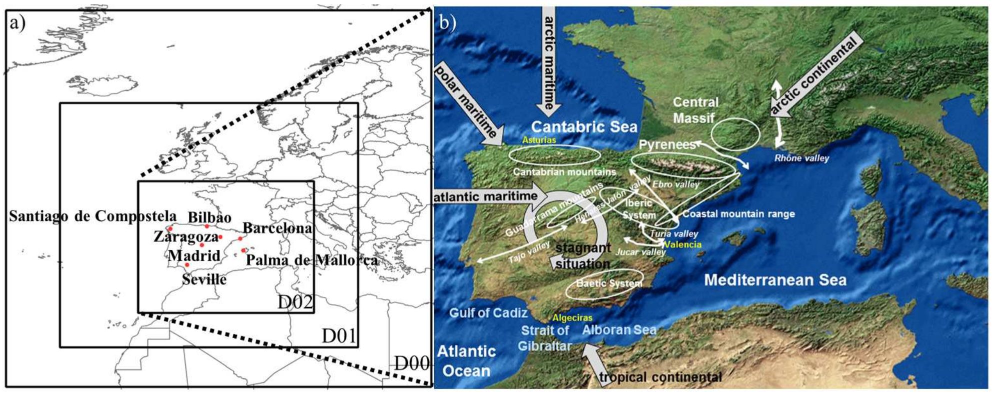

Figure 2. (a) Evaluated spatial domains. D00 (18.75N – 76.5N / 33.75W – 31.5 E), D01 (24.75N – 62.25N / 25.5W – 20.25 E), D02 (30N – 50.25N / 13.5W – 13.5 E) and origin of back-trajectories. (b) Topographic characteristics of interest. The arrows indicate the main advection of air masses towards the IP according to Martín-Vide and Olcina (2001).
538x214mm (96 x 96 DPI)

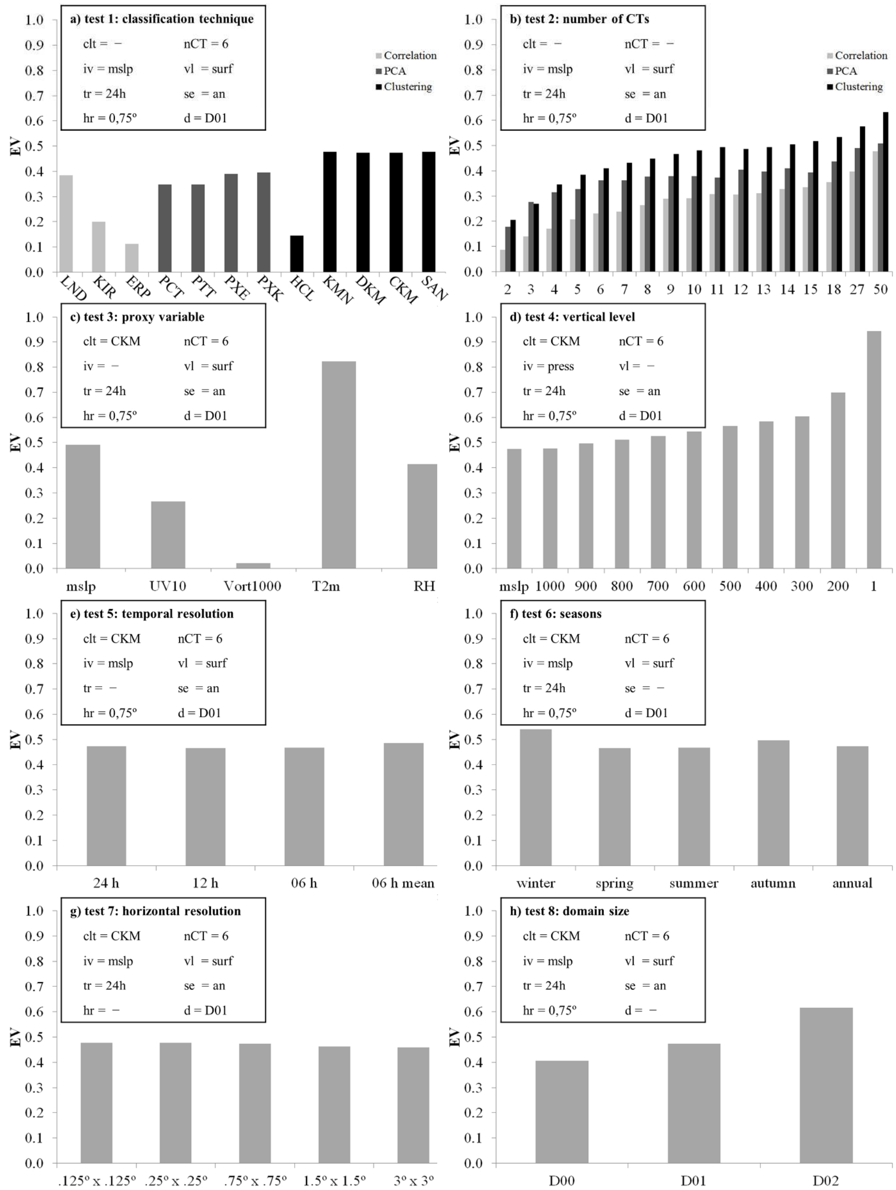

Figure 3. Results of the sensitivity tests described in Table 1 evaluated by means of the Explained Variation (EV). a) test 1, classification technique; b) test 2, number of circulation types (mean EV for correlation techniques, PCA techniques and clustering techniques); c) test 3, meteorological variable used as proxy; d) test 4, vertical level; e) test 5, temporal resolution; f) test 6, seasons; g) test 7, horizontal resolution; and h) test 8, domain size. Every single plot shows the fixed (box) and variable (bars) factor described in Table 1.
592x792mm (96 x 96 DPI)

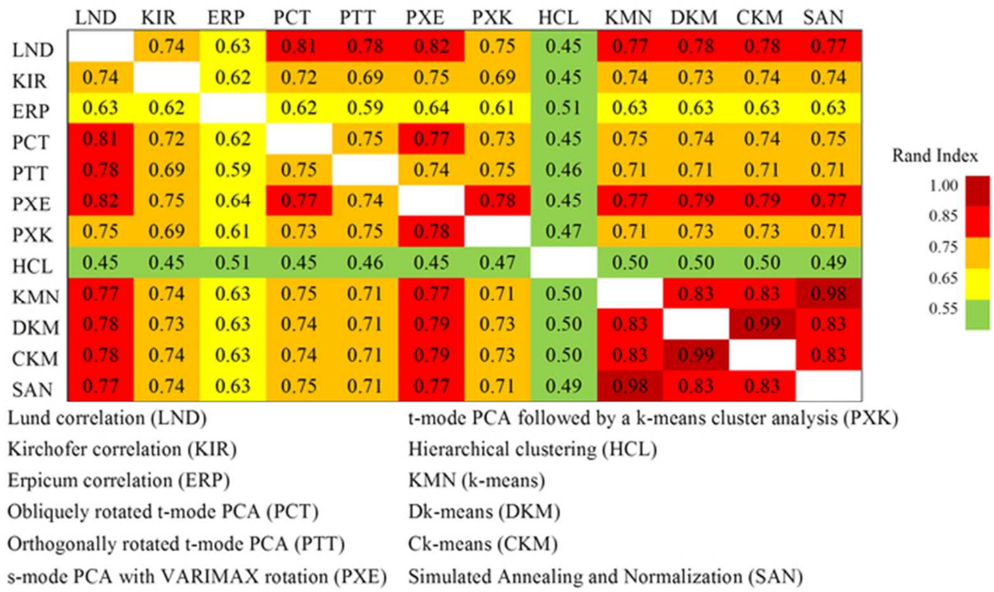

	LND	KIR	ERP	PCT	PTT	PXE	PXK	HCL	KMN	DKM	CKM	SAN
LND		0.74	0.63	0.81	0.78	0.82	0.75	0.45	0.77	0.78	0.78	0.77
KIR	0.74		0.62	0.72	0.69	0.75	0.69	0.45	0.74	0.73	0.74	0.74
ERP	0.63	0.62		0.62	0.59	0.64	0.61	0.51	0.63	0.63	0.63	0.63
PCT	0.81	0.72	0.62		0.75	0.77	0.73	0.45	0.75	0.74	0.74	0.75
PTT	0.78	0.69	0.59	0.75		0.74	0.75	0.46	0.71	0.71	0.71	0.71
PXE	0.82	0.75	0.64	0.77	0.74		0.78	0.45	0.77	0.79	0.79	0.77
PXK	0.75	0.69	0.61	0.73	0.75	0.78		0.47	0.71	0.73	0.73	0.71
HCL	0.45	0.45	0.51	0.45	0.46	0.45	0.47		0.50	0.50	0.50	0.49
KMN	0.77	0.74	0.63	0.75	0.71	0.77	0.71	0.50		0.83	0.83	0.98
DKM	0.78	0.73	0.63	0.74	0.71	0.79	0.73	0.50	0.83		0.99	0.83
CKM	0.78	0.74	0.63	0.74	0.71	0.79	0.73	0.50	0.83	0.99		0.83
SAN	0.77	0.74	0.63	0.75	0.71	0.77	0.71	0.49	0.98	0.83	0.83	

Figure 4: Rand Index matrix between classifications derived with the reference set-up and other classification techniques, calculated on a climatic basis (1983-2012).
60x36mm (300 x 300 DPI)

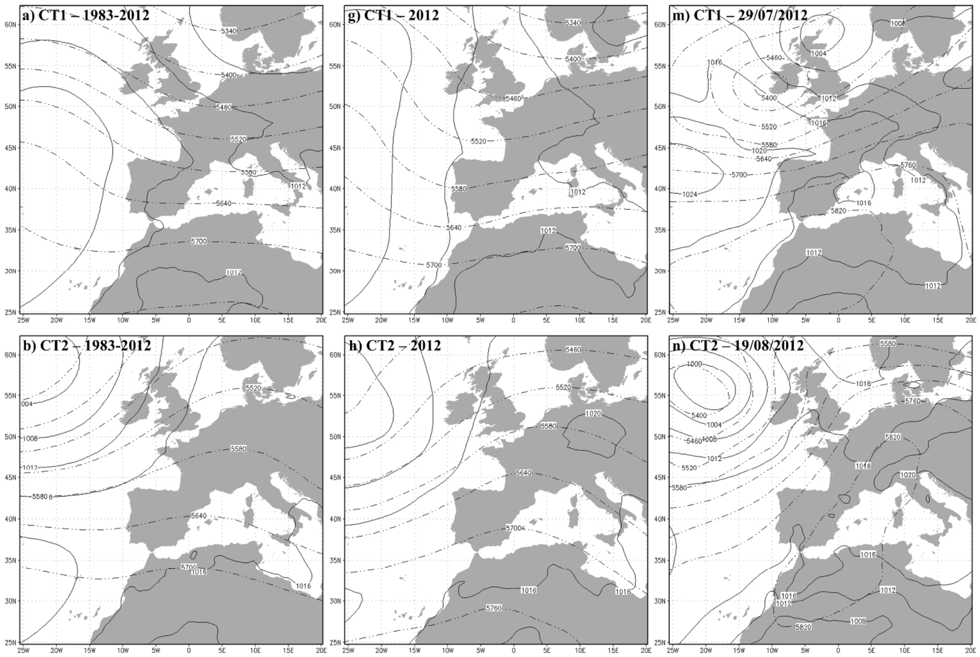

Figure 5. Circulation types derived with the reference set-up for the climatic 1983-2012 period (left), the representative year 2012 (center) and representative day of each CT (right). Solid contours show mslp isobars (hPa) and dashed-dotted contours indicate Z500 isolines (masl).
811x566mm (96 x 96 DPI)

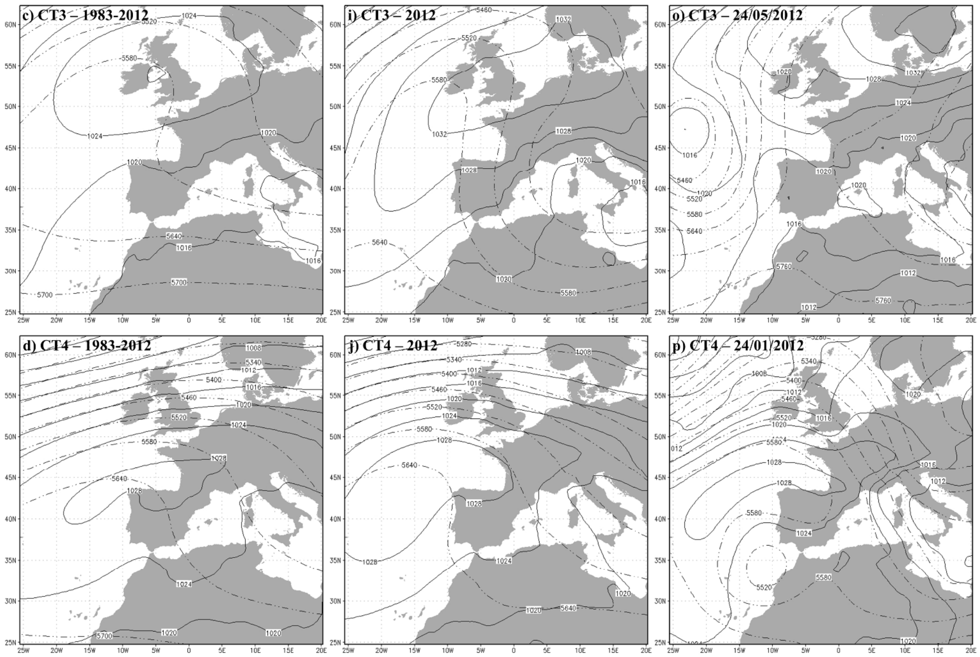

Figure 5. Continued.
811x566mm (96 x 96 DPI)

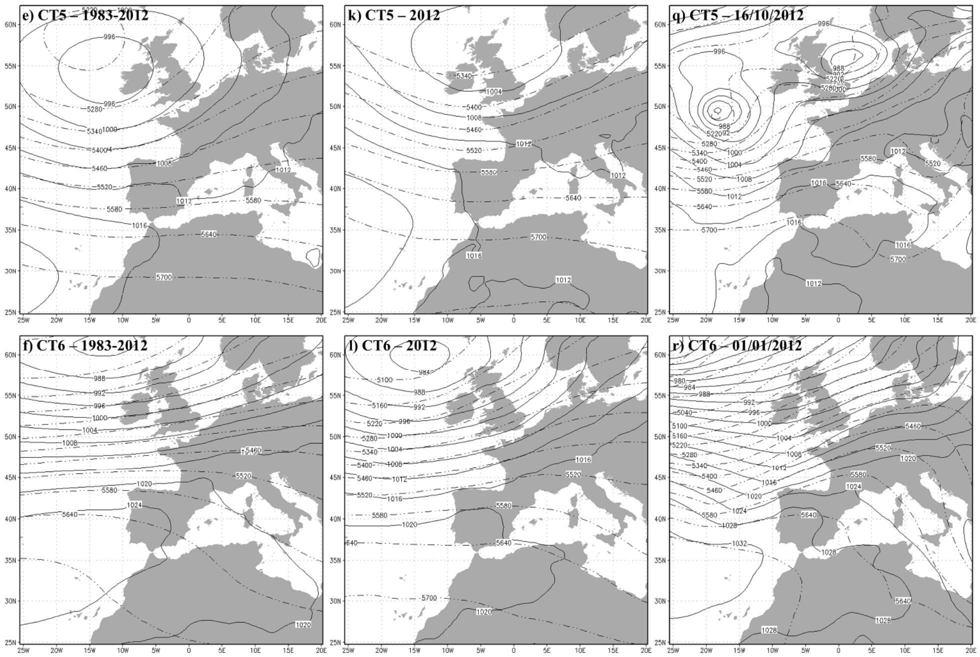

Figure 5. Continued.
811x566mm (96 x 96 DPI)

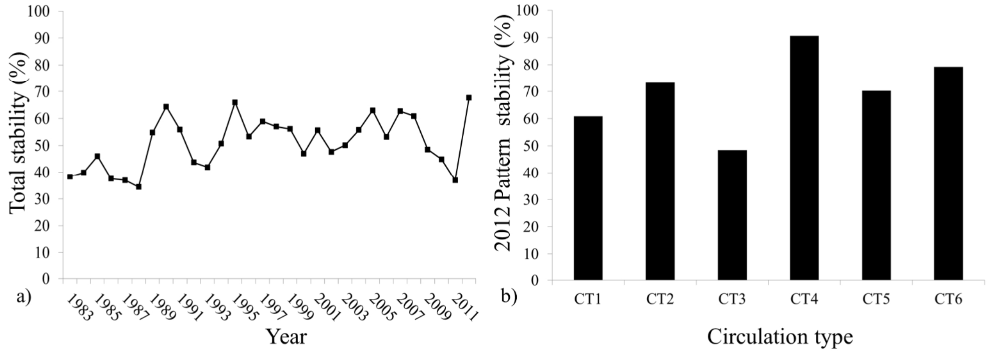

Figure 6. Temporal stability of the classification. (a) Total stability by years: yearly percentage of days classed in the same CT as in the climatic classification. (b) Stability for the year 2012: percentage of days within 2012 classes in the same CT as in the climatic classification for every CT.
642x242mm (96 x 96 DPI)

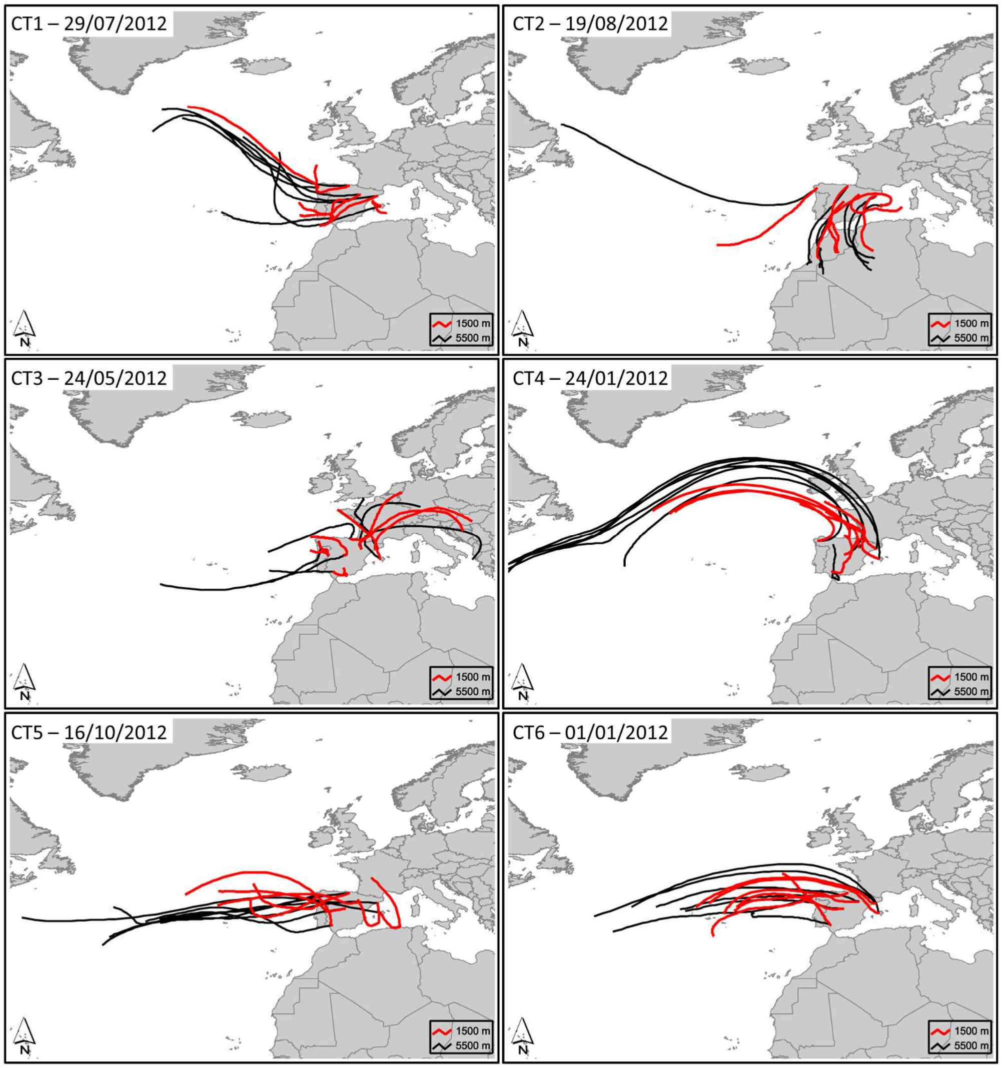

Figure 7. HYSPLIT 60 hour back-trajectories at 1500 magl (red line) and 5500 magl (black line) for representative days in 2012 corresponding to each CT: July 29th (CT1), August 19th (CT2), May 24th (CT3), January 24th (CT4), October 16th (CT5) and January 1st (CT6). The trajectories arrive at the cities of Santiago de Compostela, Bilbao, Barcelona, Zaragoza, Madrid, Seville and Palma de Mallorca (Fig 2.).
607x647mm (96 x 96 DPI)

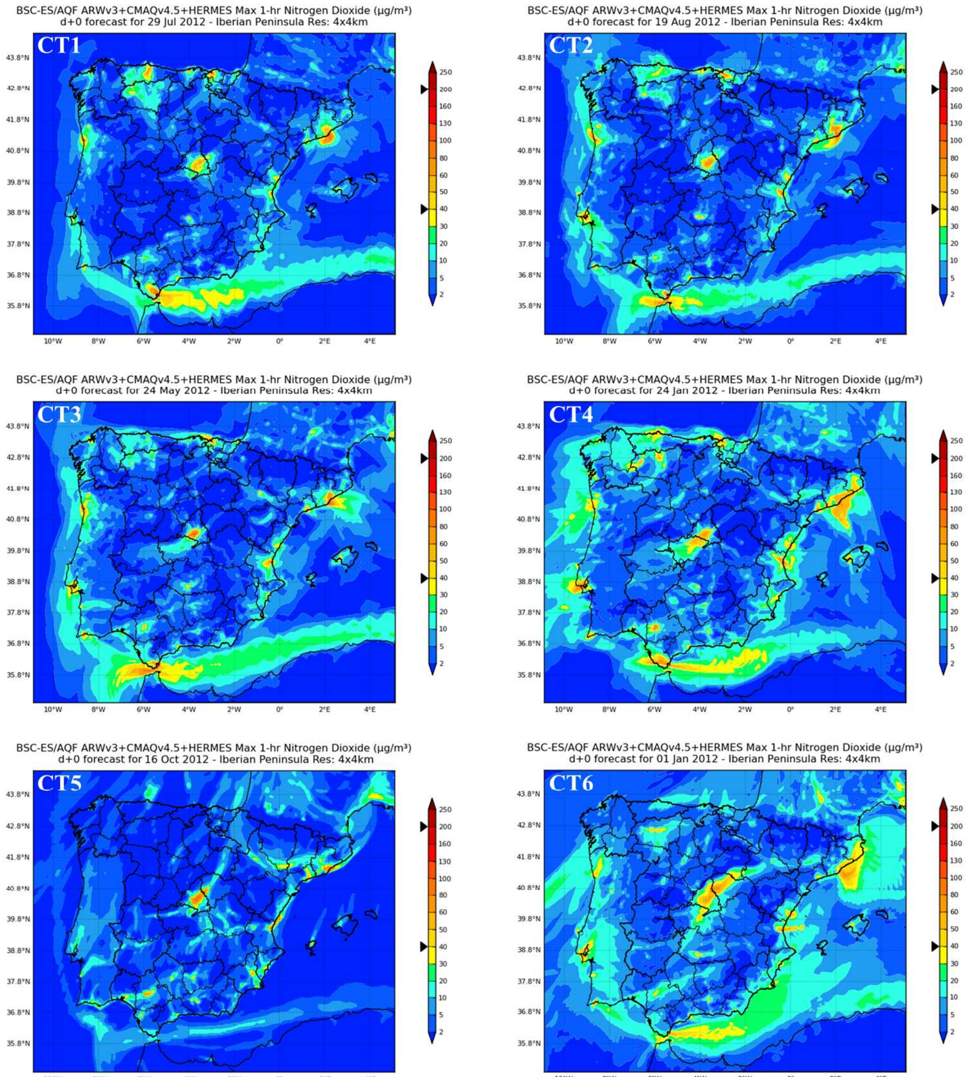

Figure 8. 1h-maximum NO_2 concentration (µg m^{-3}) maps from CALIOPE-AQFS for representative days in 2012 corresponding to each CT: July 29th (CT1), August 19th (CT2), May 24th (CT3), January 24th (CT4), October 16th (CT5) and January 1st (CT6).

481x529mm (96 x 96 DPI)

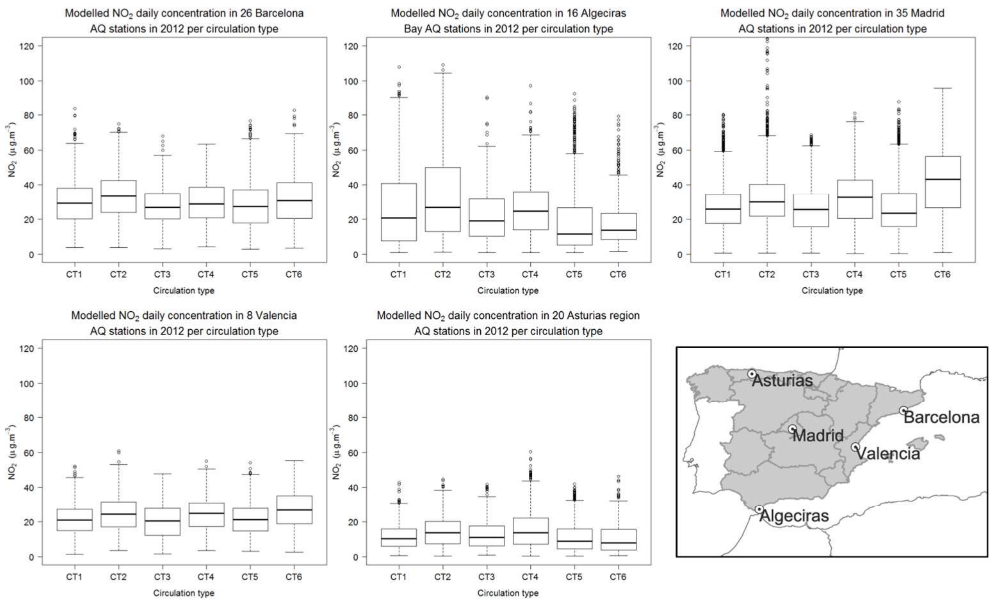

Figure 9. Daily mean NO_2 surface concentration (µg m^{-3}) of the year 2012 modelled by the CALIOPE-AQFS in points belonging to the Spanish air quality monitoring network per circulation type. The number of considered locations is 35 for Madrid, 26 for Barcelona, 8 for Valencia, 16 for Algeciras, and 20 for Asturias.
660x412mm (96 x 96 DPI)